

MULTI-SPECTRAL CLASSIFICATION OF HYDROMETEORS USING AMSU-B DATA

Corresponding author address: Abolhassan Gheiby
 Department of Physics, University of Hormozgan, Bandar Abbas-3995, Iran
 E-mail: abolhassang@yahoo.com

Abstract:

The Advanced Microwave Sounding Unit-B (AMSU-B), flying on the NOAA-15, 16, and 17 satellites, is the new generation of a series of microwave imagers/sounders that can sense atmospheric moisture and other hydrometeors through clouds. This paper demonstrates the potential of multi-frequency AMSU-B data for classifying different types of hydrometeors. Ten of these classes have been found using data (station report, radiosonde, and infrared and water vapour images) over Iran. Co-located AMSU-B data are used to perform a quantitative classification of these meteorological situations. Three main classes, heavy precipitating, moderate precipitating, and non-precipitating hydrometeors are found based on the multi-frequency brightness temperature signatures. The results suggest that the signatures of precipitating and non-precipitating hydrometeors are sufficiently reliable. The distinguishing points, for this type of analysis, are: (a) brightness temperature at 89 GHz, (b) slopes between 89 and 150 GHz and (c) cross over of brightness temperature curves at 183 GHz with respect to 89 GHz.

1. Introduction

Microwave remotely sensed measurements from meteorological satellite instruments play an important role for study earth and its atmosphere. Satellites provide valuable information on many key parameters of the global-scale hydrological cycle (water vapor, precipitation, snow/ ice crystals etc.). Simulation of brightness temperatures at the top of the atmosphere for the different microwave frequencies and role of clouds in microwave remote sensing problem has been the subject of discussion in last 20 years. Mugani and Smith (1988), Mugani et. al (1990), and Adler et al (1991) have shown that cloud liquid water significantly affects microwave T_B 's. At frequencies of 89, 157 and 183 GHz, T_B effects from cloud liquid water (Muller et. al 1992; Huang and Diak 1992, Muller et. al 1994) and measurements respond to cirrus ice cloud regarding these high-frequency microwave channels (Eyre 1990; Wilheit 1990), can be substantial. However, Muller et. al (1994) have examined Mie scattering from large liquid cloud droplets and effects of cloud ice for frequencies close to AMSU-B.

Remote sensing of different weather events using satellite data from the earlier microwave sensor are well calculated (Wilheit et. al 1976, Spencer et. al. 1983, and Lee 1994). However, the most of these microwave sensors, which are used in the earlier meteorological satellites, had coarse resolution. High spatial and temporal

resolution is generally required to define the atmospheric meso-scale phenomena. The AMSU-B reports, with 16 km resolution at nadir and six passes daily (after August 24, 2002), is an important source of data for the analyzing different weather events. AMSU-B provides information mainly about atmospheric water vapor at different frequencies dominantly related to different altitudes. It measures microwave radiation emitted by the earth and the atmosphere, at five frequencies (or channels). Channel 16 senses at 89 GHz, channel 17 at 150 GHz and channels 18-20 sense around 183 GHz water vapor band. The 89 GHz is sensitive to combination of surface temperature and surface emissivity, while the other higher frequencies are sensitive to the atmospheric constituents at increasingly higher altitudes.

The land, Ocean, and atmosphere all have different absorbing and emitting properties at different microwave frequencies. Land surface is composed of many types of substances. Therefore, they have varying emissivities. Various researches have addressed the issue of high background emissivity in the microwave portion of the spectrum. Felde and Pickle (1995) retrieved emissivity at 91 and 150 GHz over various surfaces including snow, bare soil, and vegetation using SSM/T2 data, Jones and VonderHaar (1997), and Grody N C (1998) with SSM/I data. Land surface emissivity calculations, from SSM/I in the Europe and Africa regions, have been also performed by

Prigent et. al. (1997). However, Grody (1998) has shown that the emissivities range from about 0.55 for re-frozen snow, ~0.6 for water surface, to 0.95 for dry or vegetated land at 89 GHz and to ~1.0 for air at water vapor frequencies (176.3-182.3 GHz). Each channel has a different mixture of sensitivities to these various features. In effect, the 89 GHz (channel 16) is a window frequency for O₂ and H₂O lines, and one looks at the T_B's near the ground. The 150 GHz (channel 17) is mainly for weak water absorption and sees down fairly deeply into the atmosphere. It is affected mostly by low-level atmospheric water vapor (below ~3 km). The three 183 GHz channels are for H₂O absorption peak as well as a little to either side. Channel 18 (183.3 ± 1 GHz) sees high-level moisture (about 300 hPa), channel 19 (183.3 ± 3 GHz) looks a little deeper (to about 500 hPa) and channel 20 (183.3 ± 7 GHz) sees down to 700 hPa levels, which correspond approximately to 10, 6, and 3 km respectively. In this paper, these are denoted as 182, 180 and 176 GHz, respectively. More details on the spatial resolution, corrections, and observation geometry of the AMSU-B can be

found in the NOAA KLM Users Guide (Goodrum et. al. 2000).

The purpose of this paper is to (A) demonstrate, by visual inspection of the images, that data provided by AMSU-B, when displayed pictorially, can aid the meteorologist by indicating the exact location and extent (vertically and horizontally) of different weather events even for remote station, and (B) further this is to be supported also by quantitative signatures (graphical).

2. Data

This study employs two sets of data: (A) hourly synoptic observations reported by IMO (<http://www.wunderground.com/>) and the radiosonde data compiled by the University of Wyoming, department of atmospheric sciences (<http://weather.uwyo.edu/upperair/sounding/>). From this, ten meteorological weather features have been selected as ten different events (see table 1). For all these events, total 183 reports, are selected, from where the meteorological weather events are taken.

Events	Stations	Events	Stations
1. Clear Sky conditions (CS)	28	6. Heavy Rainfall (HR)	10
2. Snow Cover regions (SC)	20	7. Snowfall (SF)	15
3. Low level Moisture (LM)	15	8. Thunderstorms (TS)	10
4. Light rain (LR)	22	9. Upper level Moisture (UM)	20
5. Moderate Rainfall (MR)	23	10. Upper level Dry (UD)	20

Table 1: Meteorological weather events (with short forms) and corresponding number of reporting stations

The clear sky conditions and snow cover are taken from IMO synoptic observations and co-located with IR METOSAT images as well. The low and upper level moisture and upper level dry

data are taken from radiosonde observations, snowfall, thunderstorm, light, moderate, and heavy rain fall data have been taken from IMO normally reported observations (Fig 1).

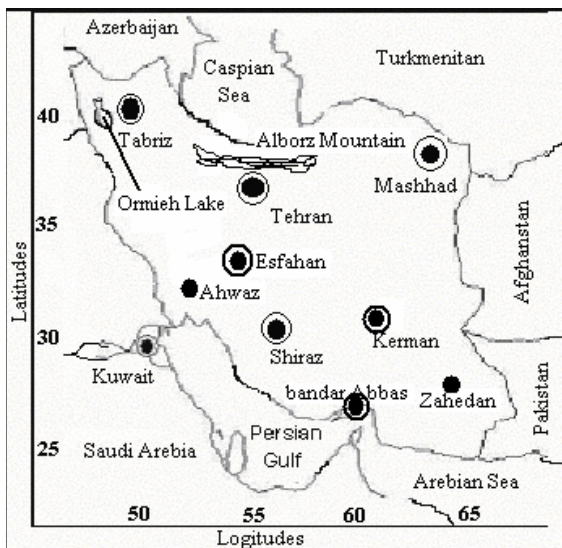


Fig. 1: geo-location of Iran and its neighborhoods. The radiosonde stations are marked by dot circles, and the IMO stations are marked by black dots with names, landmark ground-features by corresponding names.

Note that LM refers to where the relative humidity up to 700 hPa (~3 km from sea level) was more than 50%. The stations are distributed over different locations of Iran (Fig 1), and the events are distributed over different days during May 2001 to October 2002. The following limitations for the data selection have been observed: The IMO reports are available only for a few stations (only 9 stations for the study area). Some types of the events are naturally less, in the Iran region, especially heavy rain, thunderstorms, and snowfall. For example, for the snow fall only four stations (Tabriz, Tehran, Esfahan, and Mashhad) were available, because the other stations (Ahwaz, Shiraz, Kerman, Zahedan, and Bandar Abbas) are located in southern parts of Iran, which, rarely, receive snow.

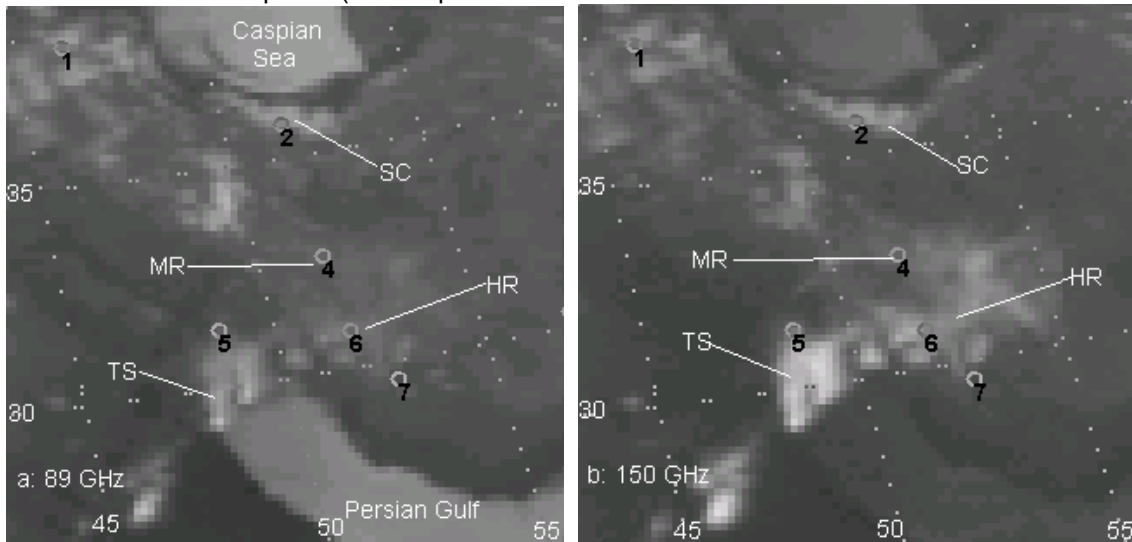
(B) The second data-set, used, is the AMSU-B level 1b data from the NOAA Satellite Active Archive (SAA). Level 1b data are radiometric calibrated brightness temperatures (T_B), and corresponding earth locations. Limitation for this data-set is due to the less time coverage of AMSU-B over the study area. It is less than 30 minutes per day (~ 5 minutes per passes).

About 150 passes of AMSU-B corresponding to the above 183 event-station reports (table 1) in (A) are available. The T_B values, only at the locations (latitudes-longitudes) of these 183 stations and close to IMO reports, are used. Except for snow cover, for all the other events, T_B data of five AMSU-B pixels (central pixel and

4 on 4 sides) have been considered. To study properties of AMSU-B frequencies in snow cover (SC) regions (over the land), data from the Alburz Mountain, in clear sky conditions, at winter season have been used. As there is no IMO report for the Alburz, the clear sky condition is co-located by IR images and nearby station (Tehran) reports. The Alburz Mountain, with about 5000 m height (Khalili 1997), is located in north of Tehran (Fig 1). During November to April, it is always covered by the snow. Thus for SC, the average T_B for six pixels (2x3) in the west-east direction (because of physical shape of Alborz mountain, which extends in west east directions) from region about 35 Km (2 pixels) north of Tehran, for 20 clear sky conditions, have been calculated.

Results

The amount of radiation measured by each AMSU-B channel is converted to T_B . As a typical example, figure 2 gives 4 frequency-channel images at 2253 UTC 07 December 2001 (i.e. 0223 IRT 08 December 2001) with all the available events marked on it (the lower T_B is whiter). Stations are indicated by the numbers on the images. For example: Tehran (2) and Shiraz (7) mist at 0220 IRT (i.e. low-level moisture), Esfahan (4) moderate rain at 0320 IRT, Ahwaz (5) thunderstorm at 0220 IRT, and Yasoge (6) heavy rain at 0330 IRT has been reported.



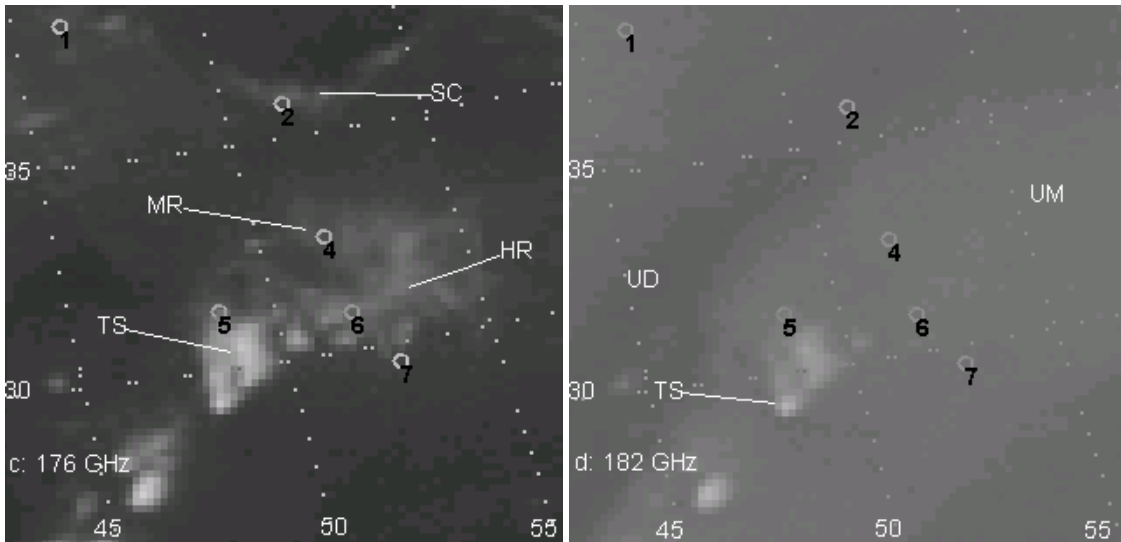


Fig 2: Four AMSU-B frequency-channel images of 08 December at 0223 IRT (i.e. December 07, 2001 at 2251 GMT) with available events marked (see table 1 for short forms). The number on the images indicate reporting stations (Tabriz=1, Tehran=2, Esfahan= 4, Ahwaz=5, Yasoge=6, and Shiraz=7). The numbers along dotted lines indicated longitudes and latitudes.

For an operational meso-scale weather forecaster, these images themselves can be a good help for knowing, *remotely, the exact locations of present thunderstorms* (limitation being the availability of the pass at the time), which is not directly observable in visible, infrared and water vapor images, obviously because of the large surrounding cloud-cover. As a matter of fact: (i) A look at the 89 GHz image give the landmarks, even without the reference to longitudes, latitudes (for example Persian Gulf and Caspian Sea in Fig 2a). The elevated snow-covered Alborz Mountain appears white gray (cold) at 89 and 150 GHz, which is due to its low emissivity of ice as compared to the land surface emissivity. It has, however, not much influence on 180 and 182 GHz channels (see Fig 2c, 2d). (ii) If white blobs are present in the image on all the 5 frequencies, they indicate thunderstorm (it is marked by TS on the four images of Fig 2). (iii) If white gray patches are seen in the images at mainly 89 and 150 GHz, they indicate near ground and low level moisture or fog or light rain (station No. 7 in Fig 2a and 2b). (iv) If white or dark flow-like streaks are seen in 180 and 182 GHz, they indicate upper level ice crystals (cirrus clouds) or upper level dry regions (UM and UD in Fig 2d), and (v) if the white blobs or patches are dominant at 150 and 170 GHz, they

may indicate mid-level clouds or mid-tropospheric rain/thunderstorm (MR and HR in the images at stations 4 and 6 (Fig 2b, 2c), respectively).

An important advantage of AMSU-B imagery is that from 89GHz image we can geo-locate ground features in spite of cirrus and altostratus shields, and further, since all AMSU-B images are co-located, the geo-location applies to all other channels as well a useful tool for operational forecaster. This is not so in other imageries such as IR, VIS and WV.

The rough descriptions have been generally verified and often used by the authors (A. Gheiby et. al 2003a, 2003b). This paper, however, attempts to give a quantitative measure of somewhat fussy statements. For this purpose, the average T_B of the five pixels (Center and four around that), for 183 stations and for five AMSU-B channels, have been calculated. First, we have taken the average T_B of 5 pixels, at each frequency separately, for the station and for the specific event. Next, the average of such averages for each channel and for each event (i.e. average T_B), over all related stations, is calculated and is presented in table 2 along with the corresponding standard deviation (σ).

Events Ch	CS	LM	LR	MR	SF	UD	UM	SC	TS	HR
1	274±2	259±2	256±1	253±1	248±2	267±1	266±2	221±6	197±7	176±2
2	278±2	262±2	255±2	248±2	244±3	273±1	269±2	225±3	168±4	178±2
3	300±1	287±2	275±1	268±2	270±2	298±1	286±1	267±1	181±5	227±2
4	273±1	268±2	258±1	255±1	254±1	278±1	262±1	266±1	187±6	247±1
5	252±1	250±2	243±1	240±1	240±1	261±1	242±1	251±3	199±8	252±1

Table 2: Average T_B (K) over all stations for the ten events of table 1, [for example 274±2 is the average of 28×5 points (pixels) see table 1] for clear sky (CS) on 89 GHz (channel 1).

The numbers 1 to 5 of the frequency-channels (Ch) in table 2 (and in all the figures) refer to channels 89, 150, 176, 180 and 182 GHz, respectively. Fig 3 gives the variation of T_B with frequency-channels for all these ten events. It can be seen from Fig 3 that these variations can be taken to be the signatures of each of these ten events, beyond 1σ . The signatures can be divided into two main groups: (a) First group is TS, HR, and SC, hereafter call as group (i), and is for the events with T_B quite low, at lower frequencies (89 and 150 GHz), for TS it is cold at all five frequencies, with quite different signatures (Fig 3). (b) The second group, mentioned above, have higher brightness temperatures, and is composed of CS, UD, UM, LM, LR, MR and SF. This group can be conveniently classified further into two

subgroups with ground brightness temperature below and above of LM. First subgroup, which is called as group (ii), contains SF, MR, and LR (with LM as reference). The second subgroup, which is called as group (iii), contains UM, UD, and CS. The events of group (ii) all are having similar trend for channel-wise T_B variation i. e. slight fall from 89 to 150 GHz, then a major rise up to 176 GHz, followed by a fall up to 182 GHz. On the contrary, the events of group (iii) show slight rise from 89 to 150 GHz, but otherwise, for the other frequencies, it is same as group (ii). For better visualization of similarities and dissimilarities between different events, differences in T_B may be more useful. Therefore, the T_B differences between the properly selected events are calculated and presented in table 3 (this is done frequency-channel wise).

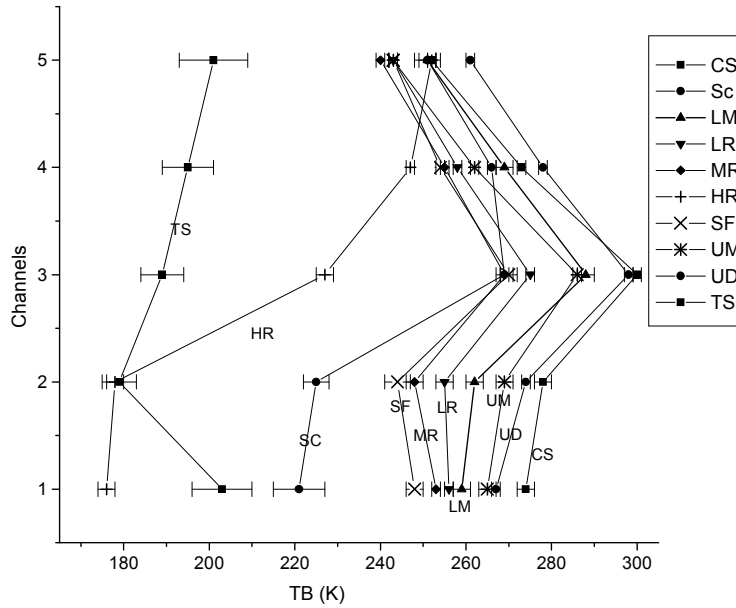


Fig 3: the average T_B for the different Hydrometeors as measured by AMSU-B (table 2).

ΔT_B Ch	LM-R	LM-MR	LM-SF	MR-SF	UM-LM	CS-UD	LM-CS	LM-UD	LM-UM
1	+3	+6	+11	+5	+7	+7	-15	-8	-7
2	+7	+14	+18	+4	+7	+5	-16	-11	-7
3	+12	+19	+17	-2	-1	+1	-13	-11	+1
4	+10	+13	+14	+1	-6	-5	-5	-10	+6
5	+7	+10	+10	0	-8	-9	-2	-11	+8

Table: 3 the brightness temperature differences between LM with group (ii) (col. 2-4), cross over events (col. 5-7), and LM with group (iii) (col.8-10).

Some points may be mentioned about data related to the curves in Fig 3: (i) AMSU-B data for thunderstorm are collected, as close as possible to the time of IMO reports (maximum within 10 minutes differences), and it is difficult to find such events, therefore number of data points for the TS is less. (ii) Data-scatters for TS are larger than the other events at all frequencies. The ranges of T_B , for TS, are 81 K (145-226K) and 71 K (151-222 K) at 89 and 182 GHz, respectively, while it is only 16 K (249-265 K) and 30 K (237-267 K) for the LM correspondingly. Error for TS is ± 7 and ± 8 at 89 and 182 GHz respectively, while for LM it is ± 2 at both 89 and 182 GHz. For 89 and 150 GHz TS may mix up with HR and SC, because of this large the basic data-scatter, but it gives a good reliability at upper frequencies (176-182 GHz). It is informative to express that the lower range in this scatter of T_B , for the TS, is related to tropical regions such as Sistan and Balochestan, south of Kerman, Hormozgan, and Bushehr provinces in spring and summer seasons, while the upper

range is related to semitropical regions like shiraz, Ahwaz, Esfahan, Tehran.

Clear sky is obviously the best data for locating ground features, and the best frequency is 89 GHz as its weighting function peaks near the ground (Muller's et. al. 1994). The most notable are the differences between dry and wet surfaces, the effect of snow cover, as well as time of the day for the data recording. Dry surface tends to have the highest emissivities and brightness temperatures, while, the wet and snow cover surface tend to have the lowest emissivity, and therefore, cools brightness temperatures when compared to dry land. Therefore, Persian Gulf and Caspian Sea, well-known landmarks in Fig.1, can be easily seen in Fig 2a. These landmarks, if not masked by clouds, are seen in 150 GHz channel (Fig 2b) also, but never seen in water vapor frequencies (Fig 2c, and 2d).

In clear sky condition, time of the day for data recorded is also an important variable that affects the T_B , in lower channels of AMSU-B. This effect is seen in different passes in Fig 4.

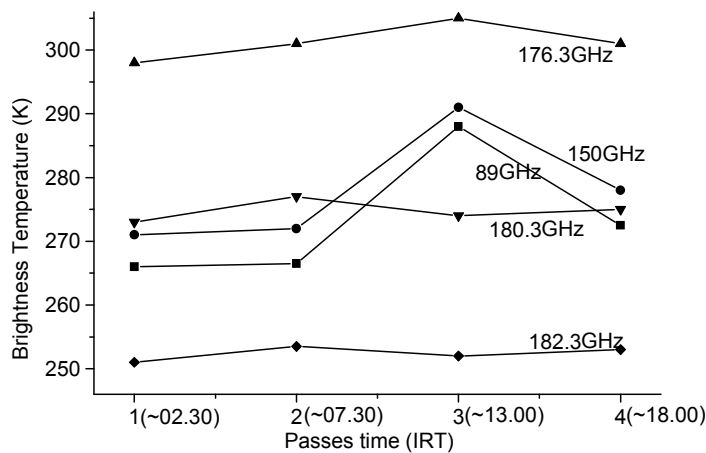


Fig 4: The T_B variations for five AMSU-B frequencies (channels) in different passes on Iran region. The IRT denote to the Iran local time.

Channels 89 and 150 GHz are more affected by time of the day. This is due to strong surface and near ground contributions of these channels. In afternoon, when the earth and its lower atmosphere becomes warm, the T_B , for lower channels (89 and 150 GHz), increases (pass 3 in Fig.4). While, at night and early morning, when the earth has become cool, the T_B is decreased (Fig 4 pass 1 and 2). The channels 176-182 GHz are not much affecting by the time of the day for data recorded, because maximum contributions to T_B , for the these channels, comes from 790 hPa (~ 2 km) and above(Muller et al 1994), which is not much dependent on time of the day. These points will help while discussing group-wise signatures below.

4. Signature discussions

The signatures of above mentioned three groups, in AMSU-B data, are described in more details and discussed in the following articles.

4.1 Group (i): The events of this group are SC, HR, and TS. Their Multi-frequency signatures are separately presented in Fig 5. It can be seen that signature differences, for the events, are very clear. At 89 GHz, the T_B values are showing that HR is coldest, next TS and then SC is warmest. HR and SC, at lower frequencies, are following similar variations of T_B , except HR is shifted to the colder values. At upper frequencies HR has opposite trend with respect to SC. it is continually increased at all frequencies, while SC from 89 to 176 GHz is increased and then from 176-182 is decreased. At 182 GHz, HR and SC are converged to the similar values. As can be seen, the maximum fall appears between frequencies 150-176 GHz. On the other hand; T_B variations for TS show fall from 89 to 150 GHz, and then smooth increase up to 182GHz. Although the 150 GHz is the best frequency, for discriminating the HR from SC, but it is not useful for discriminating the HR from TS.

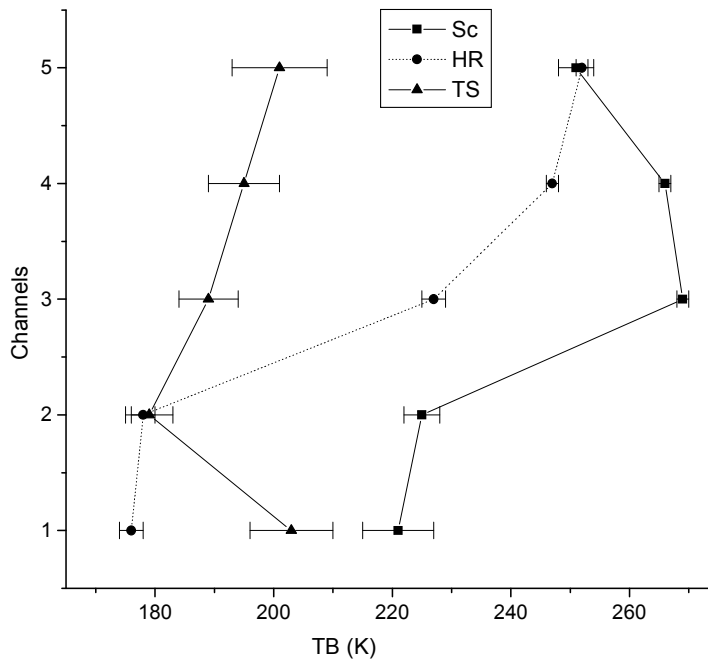


Fig 5: the average values of brightness temperatures as a function of frequency-channel for three events of group (i), SC, HR, and TS.

4.2. Group (ii):

The SF, MR, and LR belong to group (ii), all having the ground T_B (at 89 and 150 GHz) below T_B of LM (see Fig 3). Their Multi-frequency signatures (along with LM for the reference) are presented in expanded Fig 6. (a). The T_B for SF,

MR, LR, and LM, at 89 and 150 GHz, are successively increasing from *cold to warm*. (b) The main signature of this subgroup [group (ii)] is fall in T_B from 89 to 150 GHz [w. r. t group (iii)]. This followed by rise up to 176 and again a fall to 182 GHz. (c) Next though LM is nicely

separated (by $\geq 2\sigma$) from all members of this group, the group members often differ by 1σ (at 89 and 150 GHz) even less particularly at higher frequencies. (d) Signatures of SF and MR have maximum ambiguity with only one plus point,

that these two curves cross-over at lower and higher altitudes, i.e. $(T_B)_{SF} < (T_B)_{MR}$ at 89 and 150 GHz, whereas $(T_B)_{SF} > (T_B)_{MR}$ at 182 GHz. Looking at the table 3, these points become more clear.

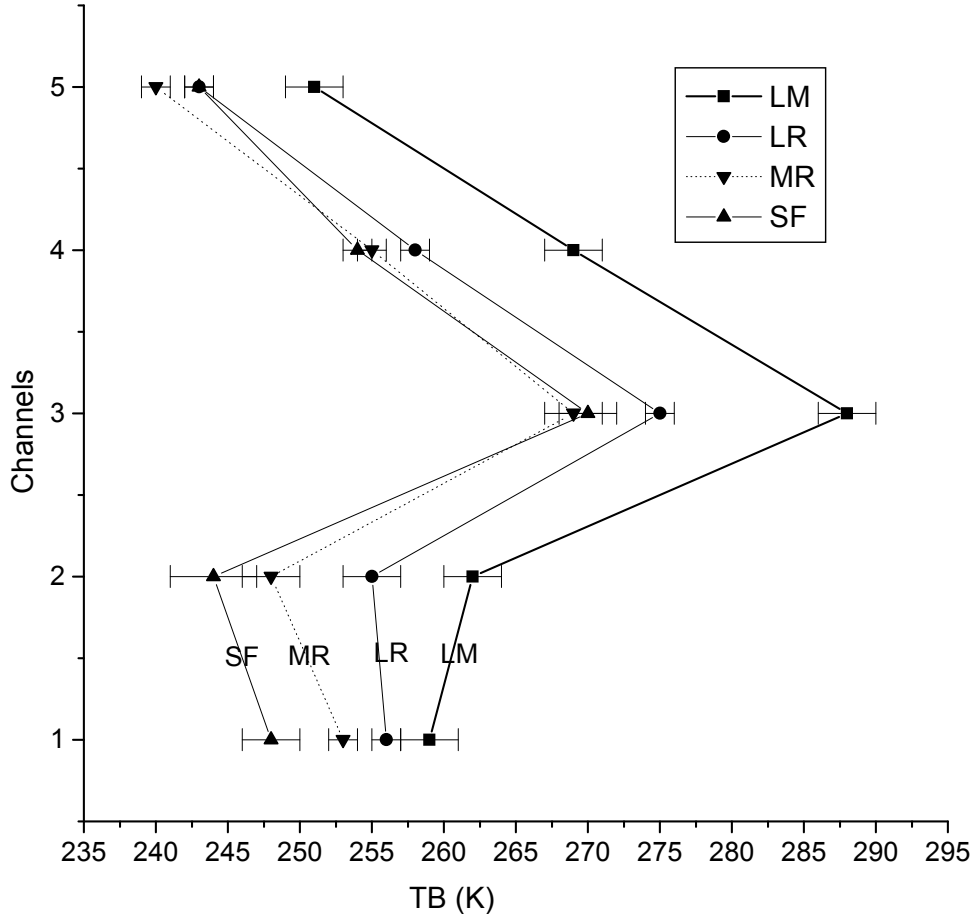


Fig 6: the average values of brightness temperature as a function of channel-frequency for three events of group (ii), LR, MR, and SF, along with LM for the reference.

4.3. Group (iii):

The events of this group are LM, UM, UD and CS, all of which have ground T_B above that of LM. Multi-frequency signatures of four events, in this group, are presented in expanded Fig 7. (a) At 89 and 150 GHz, LM, UM, UD, and CS success increasing T_B , from cold to warm. (b) As indicated above, general T_B variation, for the events of this group, is slight rise, from 89 to 150 GHz as against group (ii), and then a major rise, from 150 to 176 GHz, and then a major fall, from 176 to 182 GHz (see table 3 and Fig 7). (c) As in

case of SF and MR, the LM-UM and UD-SC curves give ambiguous. Because, at 176 GHz, they have $< \sigma$ differences (see Fig 7 and table 3 col. 5-7). However, that itself becomes the signature to distinguish them, because the curves show cross over [$(T_B)_{LM} < (T_B)_{UM}$ as well as $(T_B)_{UD} < (T_B)_{CS}$ for 89 and 150 GHz, whereas $(T_B)_{LM} > (T_B)_{UM}$ and $(T_B)_{UD} > (T_B)_{CS}$ for 182 GHz]. These points become more clear, if one looks at differences in table 3.

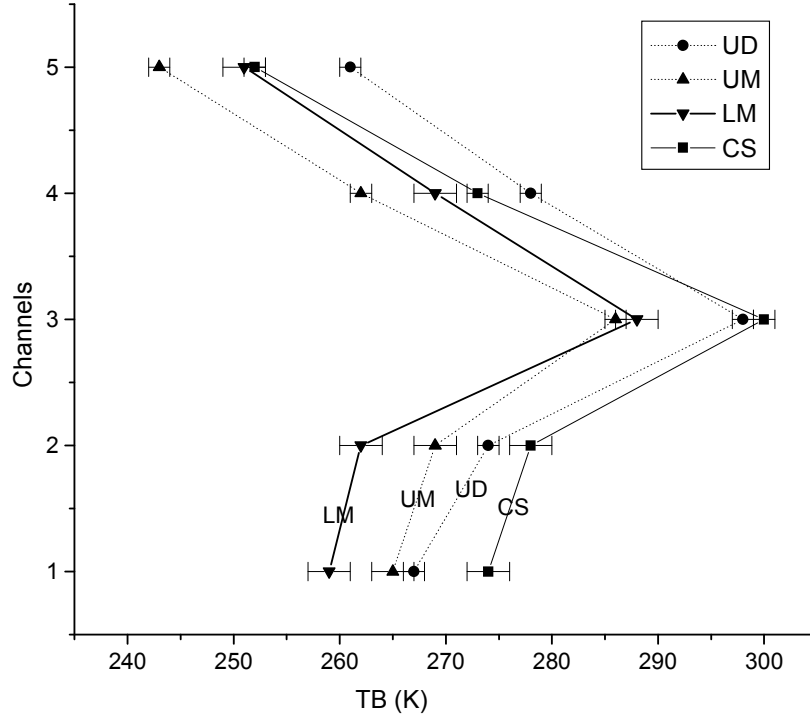


Fig 7: the average values of brightness temperature as a function of channel-frequency for three events of group (iii), CS, UD, and UM, along with LM for the reference.

5. Concluding Remarks

The ten meteorological weather events, in terms of normally used terminology in reports viz. 1) Clear Sky 2) Snow Covers regions 3) Low level Moisture regions 4) Light rain 5) Moderate Rainfall 6) Snowfall 7) Heavy Rainfall 8) Thunderstorms, 9) Upper Moisture regions, and 10) Upper Dry regions, using the available radiosonde data, IMO reports, and the corresponding AMSU-B data, are identified and averaged. The channel-wise plots are taken as the multi-spectral microwave signatures, for these ten weather events in AMSU-B data. The signatures are sufficiently reliable (almost always beyond 1σ confidence level). The distinguishing points being (a) brightness temperature at 89 GHz, (b) slopes between 89 and 150 GHz and (c) cross over of T_B curves at 183 GHz w. r. t 89 GHz. These ten events are seen to be divided into two main groups; (A) group (i) with ground T_B quite low (< 220 K) and related to more water (thunderstorm, heavy rain, and snow cover). (B) All remaining seven events appear similar with maximum T_B at 176 GHz, but with two subgroups, which are called group (ii), and group (iii). Group (ii) shows fall and group

(iii) shows rise in T_B between 89 and 150 GHz. The five AMSU-B frequencies are dominantly related to increasing altitudes, therefore, it should be remembered that these signatures are related to height-variations of water forms and concentrations.

It is felt that using these quantitative signatures one can “see remotely” the present weather situation anywhere at meso-scale (few pixels data is taken at the event-station), and hence can be of help for “operational forecasters” for his predictions, and a useful tool for air traffic planning. Shortcomings are that the AMSU-B data are available only four times a day at a place and sometimes a specific point may come in gaps in earth scanning or orbiting satellite.

The most important limitation of this analysis, however, is that the analysis is done for well-defined selected and distinguished weather events and hence has to be carefully used if weather situation is not that simple. Secondly, no time factor (wind etc.) is brought into picture. Lastly analysis is done for only one region viz. Iran and its general validity is not assumed.

Acknowledgements: The work reported in this paper was given computational support by ISRO-Cell research scheme in Department of Space Sciences University of Pune. The AMSU-B level 1b data were obtained from the NOAA Satellite Active Archive at www.saa.noaa.gov. Soundings data are obtained from University of Wyoming www.das.uwyo.edu/upperair/sounding. The ground observation data are from Iran Meteorology Organization at <http://www.wunderground.com>. The authors are thankful to these organizations for these kind help.

6. References:

Adler R. F, and I. M. Hakkarinen, 1991, Aircraft multi-frequency passive microwave observations of light precipitation over the Ocean, *J. Atmos. Oceanic Technol.*, **8**, 201-220.

Felde G. W, and J. D. Pickle, 1995, Retrieval of 91 and 150 GHz Earth surface emissivities, *J. Geophys. Res.*, **100**, 20855-20866.

Gheiby A, D. M. Puranik, P. N. Sen, A. D. Tillu, D., and R. N. Karekar, 2003a, Signatures of Rain and Thunderstorm and their Exact Locations Using AMSU-B Data Onboard NOAA-15, 16 Satellites; J. Behari, 2003a, *Microwave Measurement Techniques and Applications*, Anamaya Publishers, New Delhi, India, 265.

Gheiby A, P. N. Sen, A. D. Tillu, D. M. Puranik, R. N. Karekar, 2003b, Multi-Spectral Classification of Meteorological Features in AMSU-B Images, presented in the symposium on "Advances in Microwave Remote Sensing and Applications", CRSE, IIT Mumbai, January 21-23.

Goodrum. G, Kidwell K B and Winston W, 2000, NOAA K L M User's Guide, Online at <http://www.2.ncdc.noaa.gov/docs/klm/>

Grody N C, 1988, Surface identification using satellite microwave radiometers, *IEEE Trans. Geoscience and Remote Sensing*, **26(6)**, 850-859

Huang, H. L., and G. R. Diak, 1992, Retrieval of nonprecipitating liquid water cloud parameters from microwave data: A simulation study. *J. Atmos. Oceanic Technol.*, **9**, 354-363

Khalili M, 1997, The Climate of Iran: North, South, Kavir (Desert), Mountains, *The Transportation Industry (special travel edition)*, **7**, 48-53.

Jones A. S, and T. H. Vander Haar, 1997, Retrieval of Microwave surface emissivities over land coincident microwave and infrared satellite measurements, *J. Geophys. Res.*, **102**, 13609-13626.

Lee TF, 1994, Images of Precipitations from DMSP SSM/T-2, SSM/I and OLS, *J. Appl. Meteor.*, **34**, 788-793.

Mugani A, and E. A. Smith, 1988, Radiative transfer to space through a precipitation cloud at microwave frequencies. Part I: Model description. *J. Appl. Meteor.* **27**, 1055-1073.

Mugani A, H. J. Cooper, E. A. Smith, and G. J. Tripoli, 1990, Simulation of microwave brightness temperatures of an evolving hailstorm at SSM/I frequencies, *Bull. Amer. Meteor. Soc.* **71**, 2-13.

Muller, B. M., H. E. Fuelberg, and X. Xiang, 1992, Brightness temperature simulations for a physical interpretation of AMSU moisture channels, preprints, *Sixth Conf. Satellite Meteorology and Oceanography*, Atlanta, Amer. Meteor. Soc. 438-441.

Muller MB, Henry EF and Xiang X, 1994, Simulations of the effects of water vapour cloud liquid water and ice on AMSU moistures channel Brightness Temperatures, *J. Appl. Meteor.*, **33**, 1133-1154.

Prigent, C., W. B. Rossow, and E. Matthews, 1997: Microwave land surface emissivities estimated from SSM/I. *J. Geophys. Res.*, **102**, 21 867-21 890.

Spencer R W, Olson W S, Rongzhang W, Martin D W, Weinman J. A, and Santek D. A, 1983, Heavy Thunderstorm Observed Over Land by the Nimbus 7 Scanning Multichannel Microwave Radiometer, *J. Climate and Appl. Meteor.*, **22**, 1041-1046.

Wilheit, T. T, 1990, An algorithm for retrieving water vapor profiles in clear and cloudy atmospheres from 183 GHz radiometric measurements: simulation study. *J. Appl. Meteor.*, **29**, 508-515.

Wilheit T. T, Chang A. T. C, King J. L, Rodgers E. B, Nieman R. A, Krupp B. M, Milman A. S, Stratigos J. S and Siddalingaiah H, 1982, Microwave Radiometric Observations Near 19.35, 92 and 183 GHz of Precipitation in Tropical Storm Cora, *J. Appl. Meteor.* **21**, 1137-1145